JOURNAL OF GEOPHYSICAL RESEARCH, VOL. 115, D12124, doi:10.1029/2009JD012800, 2010

A 10 year climatology of cloud fraction and vertical distribution derived from both surface and GOES observations over the DOE ARM SPG site

Baike Xi,[1] Xiquan Dong,[1] Patrick Minnis,[2] and Mandana M. Khaiyer[2]

Received 7 July 2009; revised 18 January 2010; accepted 3 February 2010; published 29 June 2010.

[1] Analysis of one decade of radar-lidar and Geostationary Operational Environmental Satellite (GOES) observations at the Department of Energy (DOE) Atmospheric Radiation Measurement Program (ARM) Southern Great Plains (SGP) site reveals that there is excellent agreement in the long-term mean cloud fractions (CFs) derived from the surface and GOES data, and the CF is independent of temporal resolution and spatial scales for grid boxes of size 0.5° to 2.5°. When computed over a a 0.5 h (4 h) period, cloud frequency of occurrence (FREQ) and amount when present (AWP) derived from the point surface data agree very well with the same quantities determined from GOES for a 0.5° (2.5°) region centered on the DOE ARM SGP site. The values of FREQ (AWP) derived from the radar-lidar observations at a given altitude increase (decrease) as the averaging period increases from 5 min to 6 h. Similarly, CF at a given altitude increases as the vertical resolution increases from 90 to 1000 m. The profiles of CF have distinct bimodal vertical distributions, with a lower peak between 1 and 2 km and a higher one between 8 and 11 km. The 10 year mean total CF, 46.9%, varies seasonally from a summer minimum of 39.8% to a maximum of 54.6% during the winter. The annual mean CF is 1%–2% less than that from previous studies, ~48%–49%, because fewer clouds occurred during 2005 and 2006, especially during winter. The differences in single- and multilayered CFs between this study and an earlier analysis can be explained by the different temporal resolutions used in the two studies, where single-layered CFs decrease but multilayered CFs increase from a 5 min resolution to a 1 h resolution. The vertical distribution of nighttime GOES high cloud tops agrees well with surface observations, but during the daytime, fewer high clouds are retrieved by the GOES analysis than seen from the surface observations. The FREQs for both daytime and nighttime GOES low cloud tops are significantly higher than surface observations, but the CFs are in good agreement.

Citation: Xi, B., X. Dong, P. Minnis, and M. M. Khaiyer (2010), A 10 year climatology of cloud fraction and vertical distribution derived from both surface and GOES observations over the DOE ARM SPG site, *J. Geophys. Res.*, *115*, D12124, doi:10.1029/2009JD012800.

1. Introduction

[2] Clouds have been classified as the highest priority in climate change by the U.S. Climate Change Research Initiative (USCCRI, 2001; www.climatescience.gov/about/ccri.htm) because they are one of the largest sources of uncertainty in predicting potential future climate change [*Wielicki et al.*, 1995; *Solomon et al.*, 2007]. The vertical distribution of clouds impacts the vertical heating and cooling rate profiles by radiative and by precipitative and evaporative processes [e.g., *Stephens et al.*, 2002]. The assumed or computed vertical structures of cloud occurrence in general circulation models (GCMs) are one of the main reasons why the different models predict a wide range of future climates [*Stephens et al.*, 2002; *Naud et al.*, 2008]. For example, the majority of the GCMs can only simulate 30%–40% of the middle-high cloud fractions (CFs) observed in the midlatitudes by satellites, and half of the GCMs underestimate low cloud cover [*Zhang et al.*, 2005], while only a few overestimate it [e.g., *Illingworth et al.*, 2007]. Also, surface observers can see most of the low clouds with or without higher clouds above them [e.g., *Warren et al.*, 1984], while satellites can observe most of the high clouds with or without lower clouds underneath [e.g., *Chang and Li*, 2005]. These limitations hindered the development of reliable quantitative information about cloud overlap and, in general, the vertical distributions of CF and cloud occurrence.

[1]University of North Dakota, Grand Forks, North Dakota, USA.
[2]NASA Langley Research Center, Hampton, Virginia, USA.

0148-0227/10/2009JD012800

[3] The nearly continuous observations by the Department of Energy (DOE) Atmospheric Radiation Measurement Program (ARM) [*Ackerman and Stokes*, 2003] cloud radar-lidar systems can provide more accurate cloud vertical distributions and compensate for most of the shortcomings in cloud vertical distributions from both surface observers and satellite imagery. However, the limitation of such observing systems is that they view only a small column of the atmosphere above the instruments, providing only a pencil beam. How accurately the surface-based narrow radar-lidar field-of-view (FOV) observations represent the large grid boxes used in GCMs remains an unresolved issue [*Mace and Benson-Troth*, 2002] that needs to be addressed before these valuable data can be reliably used to validate GCM cloud statistics.

[4] Although the long-term continuous ARM radar-lidar observations can provide more reliable vertical distributions for verifying the GCM simulations, large-scale satellite data are critical for evaluating GCM simulated spatial distributions of clouds. For reliable application of satellite data sets in cloud processes and climate models, it is important to have a reasonable estimate of the errors in the derived cloud properties. While ground-based measurements can provide a baseline for estimating errors in the satellite products, they must first be properly analyzed and validated and their uncertainties must be understood. Comparisons between ground- and satellite-based observations must be conducted carefully because of significant spatial and temporal differences between the two observing platforms. Also, because clouds are so variable, a statistically reliable comparison requires many cloud events observed from both satellite and surface platforms. Only after we have carefully compared the satellite and surface observations can we confidently use them to validate model simulations.

[5] This paper documents fundamental statistical information about CF with various temporal resolutions and spatial scales, as well as cloud vertical distributions, using a decade of nearly continuous radar-lidar data taken from January 1997 through December 2006 at the ARM Southern Great Plains (SGP) Central Facility (SCF) site and spatially matched cloud retrievals from the eighth and tenth Geostationary Operational Environmental Satellites (GOES-8/10; hereafter GOES) taken from May 1998 through December 2006. This study primarily investigates the comparison between the temporally averaged ARM observations and the spatially averaged GOES observations. It also investigates the seasonal and vertical variations in observed clouds from both ground- and satellite-based remote sensors. The results should be valuable for comparing the observed clouds from different platforms and for enabling climate and forecast modelers to evaluate their simulations more fully over the SGP region.

2. Data and Methods

[6] The DOE ARM 35 GHz Millimeter Wavelength Cloud Radar (MMCR) [*Moran et al.*, 1998] provides continuous profiles of radar reflectivity from hydrometeors moving through the radar FOV, allowing the identification of clear and cloudy conditions. It records equivalent radar reflectivity factors (Z_e) with a 90 m vertical resolution, a total of 167 levels starting from 105 m above ground level. The MMCR uses a 3 m diameter antenna and has a 0.2° beam width, which yields a lateral resolution of 35 m at the height of 10 km for a vertically directed beam. The MMCR has four operational modes optimized for various clouds types and runs consecutively in a 36 s cycle [*Clothiaux et al.*, 1999]. The data used in this study are 5 min averages (the Mace PI product). The MACE PI product [*Mace et al.*, 2006] mimics the Active Remote Sensing of Clouds (ARSCL) product [*Clothiaux et al.*, 1999, 2000], but the key difference between the two products is how the profiles from the four operational modes are merged. For the ARSCL product, interpolation is performed on a 9 s temporal grid (the temporal spacing of the individual modes), while for the MACE PI product, *Mace et al.* [2006] estimated the most reasonable measurements for a given 90 m vertical bin from one of the modes during the 36 s cycle and assigned the three Doppler moment measurements from that particular mode to that bin.

[7] Cloud base height is derived from a composite of the Belfort laser ceilometers, micropulse lidar (MPL), and MMCR data (Cloud baseBestEstimate [*Clothiaux et al.*, 2000]). Since the laser ceilometer and lidar are sensitive to the second moment of the scatterer size distributions of the particle, rather than to the sixth moment, like the MMCR, they are virtually immune to insect contamination and precipitation particles falling below cloud base. Therefore the estimated cloud base height from the laser ceilometer and/or lidar is used as the lowest cloud base.

[8] The total CF derived from the upward-looking narrow FOV radar-lidar pair of measurements is simply the percentage of returns that are cloudy within a specified sampling time period. That is, the CF is the ratio of the number of 5 min samples when clouds were detected to the total number of 5 min samples when both radar and lidar-ceilometer instruments were working. This study uses all of the valid combined radar-lidar data, which account for ~86% of the time during the period 1997–2006. We also use this method to calculate the vertical distribution of CF, that is, the percentage of returns that are cloudy within a specified vertical resolution (90 m in this study) from 0.105 to 16 km during the 10 year period.

[9] The satellite cloud products were retrieved using algorithms developed for the NASA Clouds and Radiant Energy System (CERES) project [*Minnis et al.*, 2008a; P. Minnis et al., Cloud property retrieval techniques for CERES using TRMM VIRS and Terra and Aqua MODIS data, submitted to *IEEE Transactions on Geoscience and Remote Sensing*, 2010]. Cloud properties were retrieved from half-hourly, 4 km visible and infrared radiances taken by GOES using the four-channel visible infrared solar-infrared split-window technique (VISST) for daytime and the three-channel solar-infrared infrared split-window technique for nighttime [*Minnis et al.*, 2008a; Minnis et al., submitted manuscript, 2010]. Six cloud masks were developed to classify GOES pixels as either cloudy or clear in nonpolar [*Minnis et al.*, 2008b] and polar [*Trepte et al.*, 2002] regions during daytime (solar zenith angle (SZA) < 82°), twilight (82° ≤ SZA ≤ 88.5°), and nighttime (SZA > 88.5°). Each clear or cloudy pixel is further classified as "weak" or "strong" to indicate the degree of confidence in each pixel's classification. These masks use the 0.65, 3.9, 10.8, and 12.0 μm channels from GOES. The technique

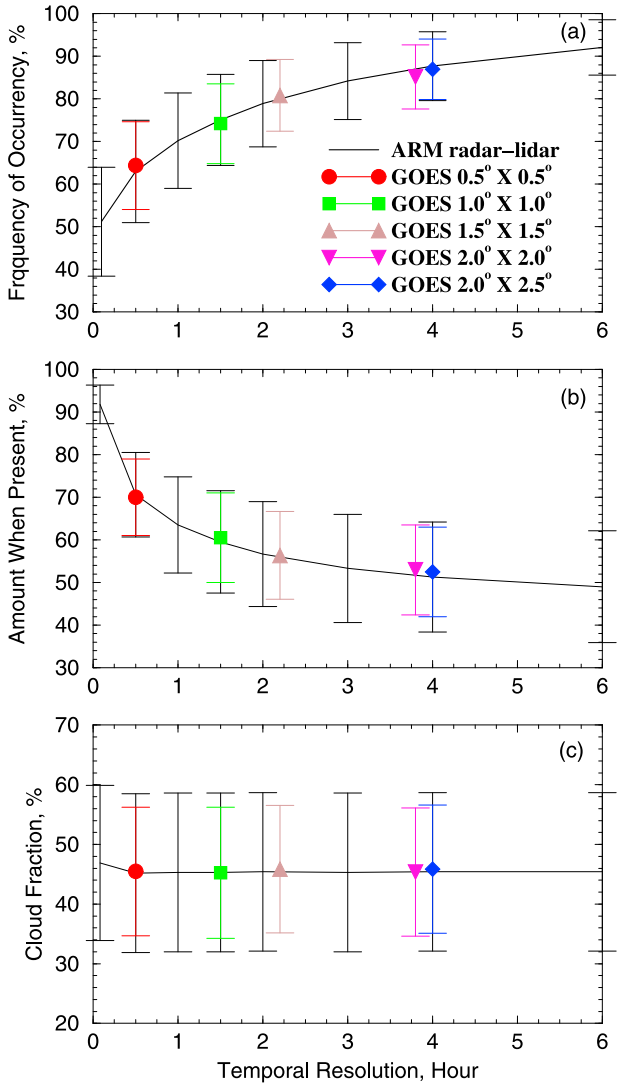

Figure 1. Dependence of (a) cloud frequency of occurrence (FREQ), (b) amount when present (AWP), and (c) cloud fraction (CF) on temporal resolutions of Atmospheric Radiation Measurement Program (ARM) surface radar-lidar observations during the period 1997–2006 and on grid boxes of satellite observations during the period from May 1998 to December 2006 at the ARM Southern Great Plains (SGP) site.

for determining effective cloud height (H_{eff}) is to estimate the effective cloud temperature (T_{eff}) based on the infrared radiance adjusted according to cloud optical depth first, and then H_{eff} is defined as the lowest altitude having T_{eff} in the vertical profile of atmospheric temperature. The profile is constructed in three parts. The rapid update cycle (RUC) numerical weather analysis model [*Benjamin et al.*, 2004] profile is used for pressures $p < 500$ hPa. The profile for $p > 700$ hPa is specified using a −7.1 K/km lapse rate anchored to the 24 h running mean surface temperature from the RUC, while a linearly weighted blend of the RUC and lapse rate is used for intermediate pressures. *Dong et al.* [2008] demonstrated that the lapse rate approach is more reliable for assigning cloud-top height from T_{eff} for boundary-layer clouds than using the soundings from either sparse radiosonde measurements or numerical weather analyses.

[10] The areal fraction of clouds, or the amount when present (AWP), is the ratio of the number of pixels classified as cloudy to the total number of pixels within a specified area (0.5° × 0.5° or 2.0° × 2.5°) centered on the SCF. The cloud frequency of occurrence (FREQ) derived from satellite observations is defined as follows. The FREQ is 0 for clear sky and 1 when AWP > 0.05. The threshold of AWP > 0.05 is used to remove the GOES observational noise and retrieval errors because more clouds occur for very small instantaneous AWP, <0.05 (for more details, see *Kennedy et al.* [2010]). The monthly averaged AWP is the average of all AWPs (>0.05 only) and represents the average cloud amount when clouds are present. The average FREQ is the ratio of the number of times when AWP > 0.05 to the total number of satellite observations during that month. Finally, the monthly mean CF (or coverage/amount), following *Warren et al.* [1984] and *Hogan et al.* [2001], is defined as the product of the monthly averaged AWP and FREQ. Note that FREQ and AWP are fundamental variables for representing cloud occurrence either in a certain time period (e.g., hour, month, season) or over a particular grid box (e.g., 0.5° × 0.5° or 2.0° × 2.5°). FREQ represents the probability of how often the clouds appear within either the time period or the area, and AWP represents how much of the area is covered by clouds for the same specified temporal and spatial domains.

[11] The FREQ, AWP, and CF derived from ARM radar-lidar pair observations are defined in the same manner as for the GOES observations but are temporally averaged values. Because both radar and lidar produce narrow FOV observations, their instantaneous observed AWP should be unity for cloudy and 0 for clear sky, and their corresponding FREQ values are 1 and 0, respectively. However, AWP decreases and FREQ increases with increased averaging temporal resolution as demonstrated in Figure 1.

[12] Because there are significant temporal and spatial differences between surface and satellite observations, comparisons between them must be conducted carefully. If there are enough samples, then the temporally averaged surface observations (a pencil beam) should be equivalent to the spatially averaged satellite results (a grid box), assuming that the satellite and surface instruments are equally efficient at detecting cloudiness. By varying the temporal and spatial resolutions, it should be possible to determine the time and space scales that can be represented by the point measurements. Therefore, we develop the following conceptual model:

$$\lim_{\text{area}\to 0} F(\text{area}) = F(\text{point}), \tag{1a}$$

$$\frac{W(h)V(h)\int_0^{\text{hours}} dt}{\text{Area}} = F(\text{area}), \tag{1b}$$

where F represents AWP in a certain period, $V(h)$ and $W(h)$ represent the mean wind speed and the width of the radar FOV at an altitude h, and area is the geometric area ($W(h) \times L$, where L is the length of the grid box used in this study). Here F(point) represents the temporally averaged radar-lidar observations, and F(area) represents the spatially averaged GOES observations. Equation (1a) indicates that the satellite

observations can match the surface point observations if the satellite grid box can be reduced to a point, while equation (1b) illustrates that the integration of the surface point observation over a certain period can represent the satellite observations.

[13] Equation (1b) illustrates that, when comparing the satellite- and surface-based quantities, there is always some mismatch in terms of the actual portions of the clouds that are sampled. The time average of the cloud samples by the small-beam radar and variable FOV (which depends on the cloud base height) is assumed to provide a value that is represented by the spatial average of the relatively large imager pixels. A more precise match of the data could have been attempted by using "wind strips" of satellite pixels. Those strips of pixels correspond to the clouds advecting over the site during the averaging period of the surface instruments. As found by *Dong et al.* [2002], however, the more precise "strip" approach yields nearly the same statistics as the simple "box" average used here, presumably because there is no assurance that the relatively large pixels are represented by the beam averages on a one-to-one basis. Thus, the GOES results averaged over the grid boxes in this study should be suitable for making the comparison with the temporally averaged surface observations as demonstrated in equation (1b).

3. Comparison of Clouds Derived with Atmospheric Radiation Measurement Program (ARM) and Geostationary Operational Environmental Satellite (GOES) Observations

[14] Figure 1 shows the means and standard deviations of FREQ, AWP, and CF with different temporal averaging resolutions, such as 5 min, 0.5 h, and 1–6 h of ARM radar-lidar observations during the 10 year period. The 5 min FREQ, AWP, and CF are the highest temporal resolutions used in this study, and other results are averaged from the 5 min observations. As demonstrated in Figure 1a, the mean FREQ rises rapidly with increased temporal averaging periods from the 5 min (51.2%) to the 6 h (92.1%) intervals, but their corresponding standard deviations drop from 12.8% to 6.5%. This is reasonable because the possibility of cloud occurrence over a longer time period is certainly higher than that over a short time period at a fixed point, but this may not be true for AWP. The mean AWP decreases with the increased averaging periods from 91.8% at 5 min to 49% at 6 h with nearly the same standard deviation. The CF (=AWP × FREQ), however, is almost constant for different temporal resolutions as shown in Figure 1c. To provide more detailed information for climate modelers, the following empirical formulae were derived to relate FREQ and AWP to temporal resolution X (hours) based on the 10 year ARM observations:

$$\begin{aligned} \mathrm{FREQ} &= 9.322\ln X + 72.5, \quad \mathrm{corr} = 0.989, \\ \mathrm{AWP} &= -7.56\ln X + 64.23, \quad \mathrm{corr} = 0.975. \end{aligned} \tag{2}$$

Figure 1 also shows the means and standard deviations of FREQ, AWP, and CF averaged from the 0.5° × 0.5° to the 2.0° × 2.5° GOES grid boxes. The FREQ, AWP, and CF derived from the 0.5° × 0.5° GOES grid box represent the smallest spatial scale used in this study, and other results from different grid boxes are averaged from half-hourly 0.5° observations. Note that the GOES results are spatially averaged, while the surface results are temporally averaged. As illustrated in Figure 1 the mean FREQ and AWP averaged from the 0.5° × 0.5° GOES grid box agree very well with the 0.5 h ARM observations, while those averaged from the 2° × 2.5° grid box are nearly the same as the 4 h surface averages. The GOES CFs derived from all grid boxes are almost the same and are in excellent agreement with the different temporal averages of surface observations as demonstrated in Figure 1c. This result indicates that the CF is independent of temporal resolution and spatial scale, and the long-term CFs derived from different temporal resolutions of surface observations can represent the areal CFs averaged from different GOES grid boxes provided that there are enough samples.

[15] To check further the validity of the conclusion drawn from Figure 1, we also plotted data for Figure 1 (not shown here) by using the individual months, seasons, and years of ARM and GOES observations which resulted in the following statistics. The FREQ values calculated from a year of observations match 88% of the relationships in Figure 1 or equation (2), while those from a season and month are 59% and 45%, respectively. Therefore, a minimum of 1 year of continuous data is required to produce the relationships (0.5 h versus 0.5° grid box and 4 h versus 2.5° grid box) in Figure 1.

[16] To analyze the spatial and temporal relationships further, the 0.5 and 4 h surface averages of FREQ, AWP, and CF are plotted against the 0.5° and 2.5° GOES means in Figure 2. Each circle in Figure 2 represents a monthly mean between May 1998 and December 2006 when both surface and satellite data are available. The monthly mean surface-derived FREQ (Figures 2a and 2d) and AWP (Figures 2b and 2e) are highly correlated with their respective GOES means and, on average, differ from the satellite means by no more than ±1.5%. The mean difference in FREQ between the 4 h surface average and the 2.5° satellite results is small, but the correlation is relatively weak, presumably owing to a small variation range (70%–98%). All of the monthly mean CFs in Figures 2c and 2f are nearly the same, and the surface and satellite values are highly correlated.

[17] The comparisons in Figure 2 beg the question: What point observations can be directly compared with satellite observations? As shown in Figures 1 and 2 the long-term mean CF is independent of temporal and spatial resolutions, and the surface-derived CF (a pencil beam) can represent the satellite-derived CF (a grid box) no matter how long the temporal average from surface observations and how large the grid box averaged from satellite observations, provided that there are enough samples. However, the AWP and FREQ derived from surface and satellite observations cannot be compared directly. The surface results must be averaged over a certain time period to match a fixed grid box of satellite observations, such as 0.5 h versus 0.5° × 0.5° grid box and 4 h versus 2° × 2.5° grid box as demonstrated in this study.

4. Cloud Vertical Distributions

[18] The relationships of FREQ, AWP, and CF in Figures 1 and 2 also elicit the following two questions: Would the

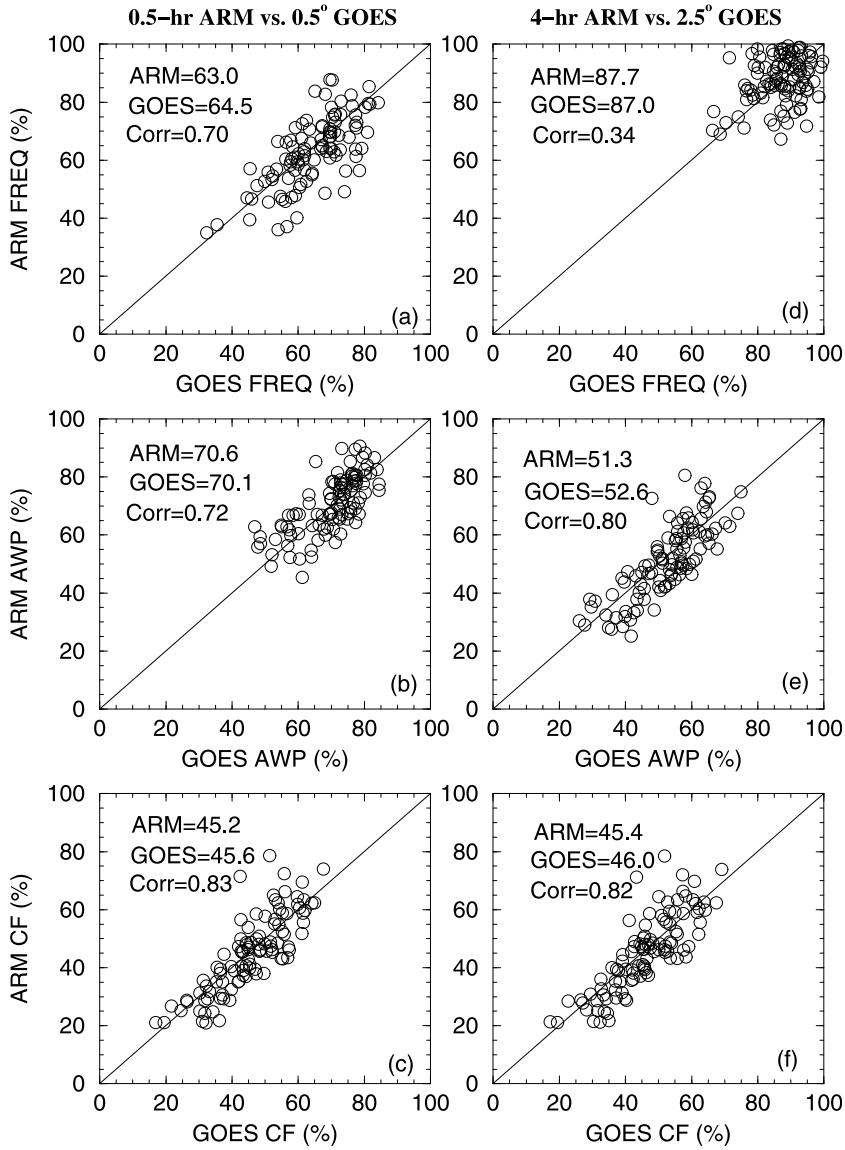

Figure 2. Scatterplots of monthly averaged (a, d) cloud FREQ, (b, e) cloud AWP, and (c, f) CF derived from Geostationary Operational Environmental Satellite (GOES; 0.5° and 2.5° grid boxes) and ARM radar-lidar observations (0.5 and 4-h averages) at the ARM SGP site, May 1998 to December 2006.

vertical distributions of FREQ, AWP, and CF change with different temporal and vertical resolutions? and Could we have the same good agreement in section 3 if we compare the highest cloud-top heights derived from ARM radar and GOES observations? In this section we attempt to answer these two questions, investigate their seasonal variations during the 10 year period, and compare these results with previous studies, such as *Dong et al.* [2006], *Kollias et al.* [2007], and *Mace and Benson* [2008].

4.1. Cloud Vertical Distributions Derived from ARM Radar-Lidar Pair Observations

[19] To explore the vertical distributions of FREQ, AWP, and CF and their dependence on different temporal resolutions, we plot Figure 3 using the 10 year ARM radar-lidar observations with a 90 m vertical resolution and four temporal resolutions, 5 min, 1 h, 3 h, and 6 h, to mimic most of the GCM or weather forecast model outputs [*Hogan and Illingworth*, 2000]. The vertical distributions of FREQ, AWP, and CF are defined the same as those in section 2 and Figure 1 but within a specified vertical resolution (90 m) from 0.105 to 16 km during the 10 year period. As demonstrated in Figure 3, although the FREQ and AWP from different temporal resolutions have similarly shaped vertical distributions, the FREQ values increase and the AWP values decrease as the averaging period increases from 5 min to 6 h. Again, the long-term mean CFs are independent of the temporal resolutions. The results shown in Figure 3 are consistent with those in Figure 1.

[20] To explore further the dependence of CF on different vertical resolutions, we plot the vertical distributions of CF using a 5 min temporal resolution and four vertical resolu-

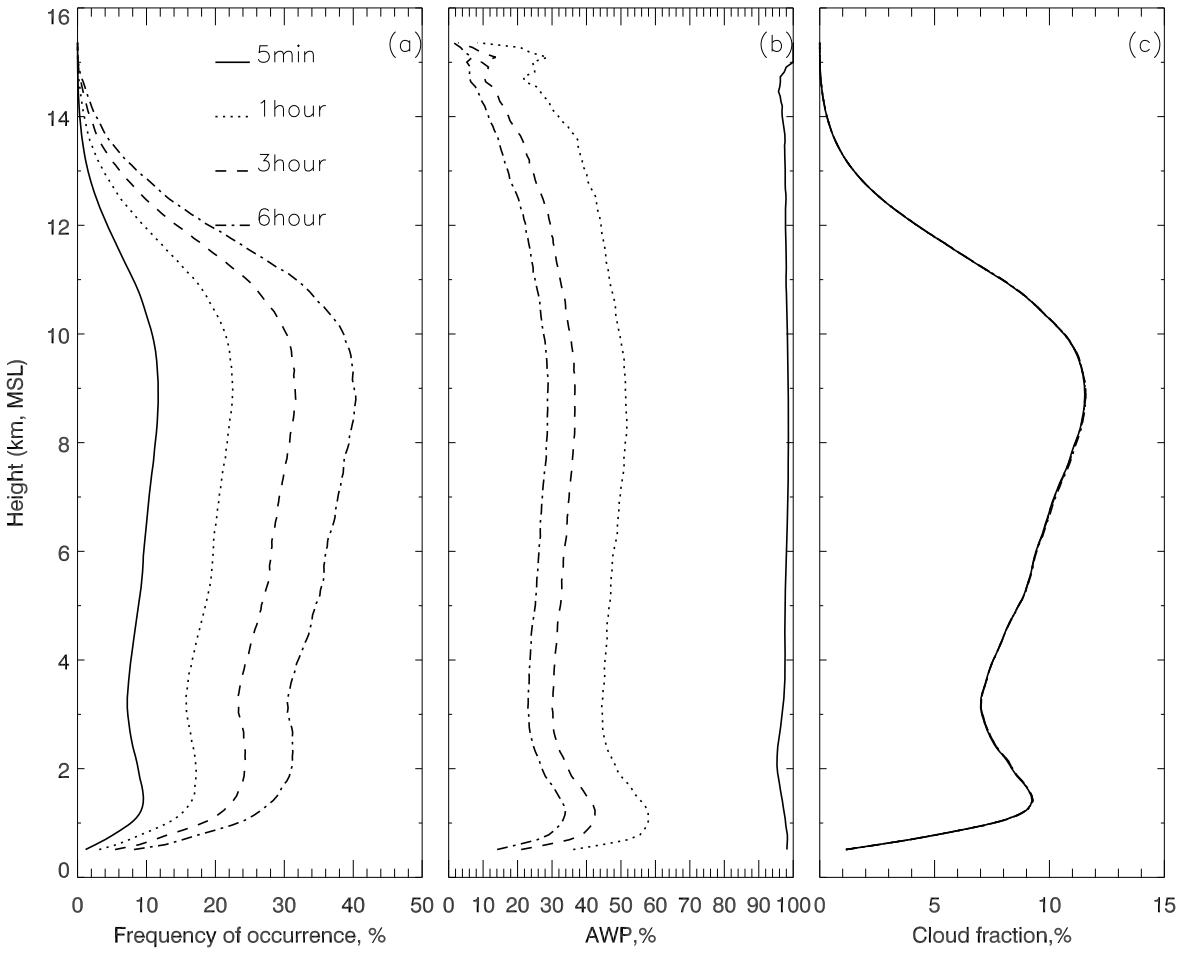

Figure 3. Mean vertical distributions of (a) FREQ, (b) AWP, and (c) CF derived from the ARM radar-lidar pair observations with a vertical resolution of 90 m and temporal resolutions of 5 min, 1 h, 3 h, and 6 h at the ARM SGP site, 1997–2006.

tions, 90 m (same as Figure 3c), 250 m, 500 m, and 1000 m, in Figure 4. As demonstrated in Figure 4 the CFs increase from 90 to 1000 m vertical resolutions at any altitude, which makes physical sense because more clouds occur at 1000 m than at 90 m vertical resolution. Figure 5 shows the annual (same as Figures 3c and 4) and seasonal mean vertical distributions of CF derived from the ARM radar-lidar observations during the period 1997–2006. The CF profiles have a relatively large seasonal variation, with the maximum values below 9 km in winter and a minimum in summer. The vertical distributions are bimodal, with a lower peak between 1 and 2 km and a higher one between 8 and 11 km. The greatest altitude of the upper-level maximum occurs around 11 km during summer as a result of the deeper troposphere and more convective storms. The low-level relative maximum during summer is not as strong as those during other seasons because stratus clouds are least common during the summer [*Dong et al.*, 2005]. The lower and upper peaks during spring and fall are the same as those for the annual mean vertical distributions and are located at ~1.3 and 8.8 km mean sea level, respectively.

[21] The ARM radar-lidar-derived CFs are further classified into 10 categories (see Figure 6 and summary in Table 1) that should represent different cloud formation and dissipation processes and different large-scale dynamics. To be consistent with *Dong et al.* [2006], we used the same definition of the single-layered clouds in this study. The single-layered low-level CF_L is the fraction of time when low clouds ($Z_{top} < 3$ km) occur without clouds above them. The high-level CF_H is determined for clouds having a Z_{base} higher than 6 km with no clouds underneath, while middle clouds (CF_M) range from 3 to 6 km without any clouds below and above. To provide more cloud types for modelers, we also adopt the *Hogan and Illingworth* [2000] method to define contiguous (C) and noncontiguous (N) clouds. Contiguous clouds are layers between which all layers are cloudy, and they cross the boundaries between the different levels, that is, altitudes of 3 and 6 km. For example, the ML-C, HM-C, and HML-C in Figure 6 are called contiguous clouds in this study. Noncontiguous clouds do not cross layer boundaries, such as the ML-N, HM-N, and HML-N. The percentages in Table 1 are CFs, the same as those in Figure 5. The annual and four seasonal (spring, summer, fall, and winter) mean total CFs are 46.9%, 50.4%, 39.8%, 43.3%, and 54.6%, respectively, indicating that there

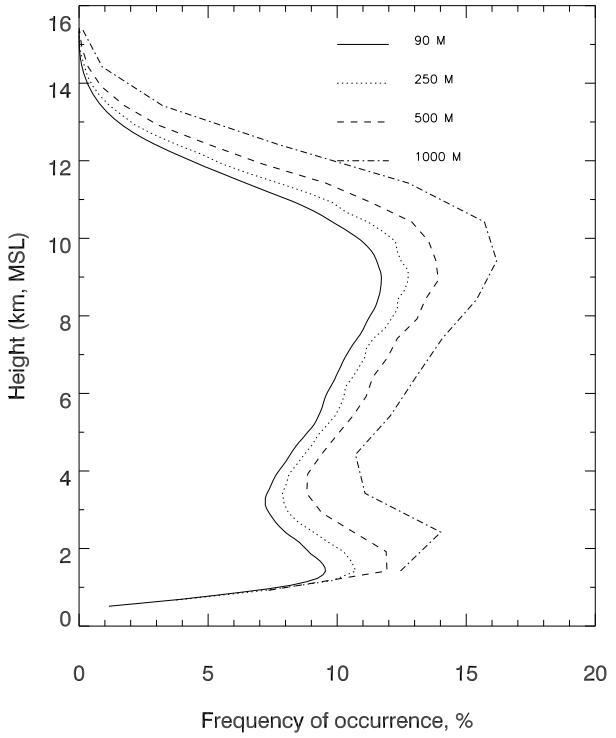

Figure 4. Mean vertical distributions of CF derived from the ARM radar-lidar observations with a 5 min temporal resolution and vertical resolutions of 90, 250, 500, and 1000 m at the ARM SGP site, 1997–2006.

are more clouds during winter and spring than during summer and fall.

4.2. Comparisons With Other Studies

[22] To determine how well the results analyzed in this study represent the cloud climatology at the ARM SCF, it is necessary to make comparisons with previous studies (e.g., *Kim et al.* [2005] and *Dong et al.* [2005, 2006], hereafter D06; *Kollias et al.* [2007], hereafter K07; and *Mace and Benson* [2008], hereafter MB08). Since the data sets used in this study and in D06, K07, and MB08 are nearly the same, we focus on the comparisons among these four studies to investigate their similarities and differences. The MACE PI products were used in all studies except for K07, which used the ARM ARSCL data for the period January 1998 to June 2004. The time periods are 1997–2002 in D06 and 1997–2004 in MB08. Although the total CFs in D06, K07, and MB08 were derived from different data sets and time periods, they have almost the same annual mean, ~48%–49%, a value that is about 1%–2% higher than that in this study. This apparent discrepancy results from the inclusion of data from 2005 and 2006, when the total CFs in 2005 and 2006 were approximately 41%. Without those 2 years the mean total CF here would be 48.5%.

[23] The vertical distributions of CF in MB08 (their Figure 2) and this study are almost the same, except that the CF is larger by ~2% in MB08, presumably because of the lower CFs during the years 2005 and 2006 included here. To compare our results (Table 1) with those in D06 and K07, we list the seasonal and annual single-layered low (CF_L), middle (CF_M), and high (CF_H) CFs, as well as their total CFs (CF_T), in Table 2. The CF differences between D06 and this study are within 2% for the annual mean and are up to 6% during winter, indicating that more clouds occurred during the winter seasons of 1997–2002 than in those of 2003–2006. These differences are due to deficits in single-layered low cloud cover during the latter period. Note that the data sets and processing methods are the same in D06 and this study except for the periods such as 1997–2002 in D06 and 1997–2006 in this study.

[24] The single-layered and total CFs during the entire average year, summer, and winter in K07 are also listed in Table 2. The total CFs of annual and summer season in K07 are 2.2% and 2.9% greater than those in this study, however, all the K07 single-layered CFs are lower than those in this study. The total single- and multilayered CFs in K07 are 22.9% and 20.1%, respectively, during the period January 1998 to June 2004. Using the same definitions as in K07, the total single- and multilayered CFs in this study are 28.8% (sum of cloud types 1–3) and 18.1% (sum of cloud types 4–10), although the contiguous CFs (cloud types 4–6) should be technically classified as single-layered clouds. There are two likely reasons for the differences between these two studies. First, the 6.1% precipitation in K07 was included as single- or multilayered clouds in this study. To

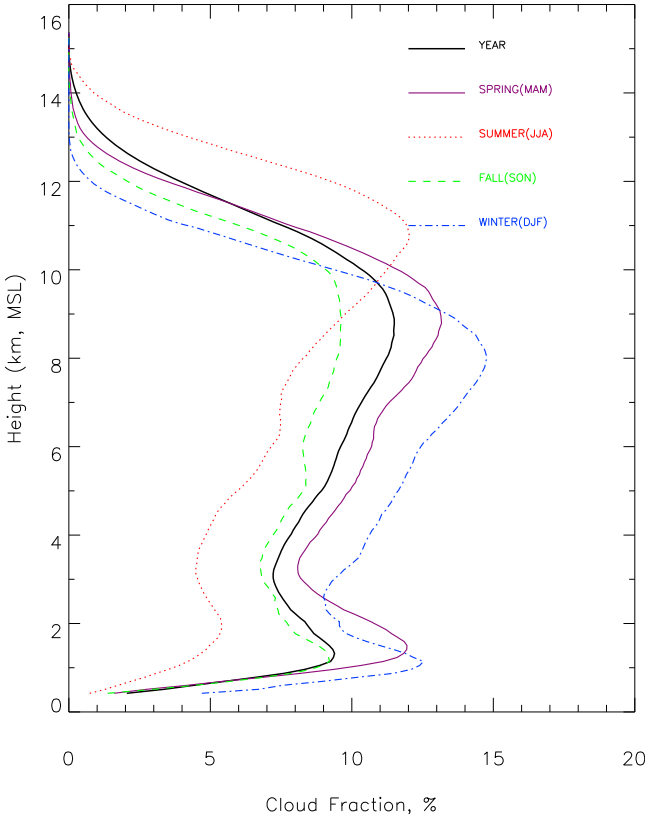

Figure 5. Mean vertical distributions of CF derived from the ARM radar-lidar observations with a vertical resolution of 90 m and a temporal resolution of 5 min at the ARM SGP site, 1997–2006. Four seasons are defined as winter (December–February), spring (March–May), summer (June–August), and autumn (September–November).

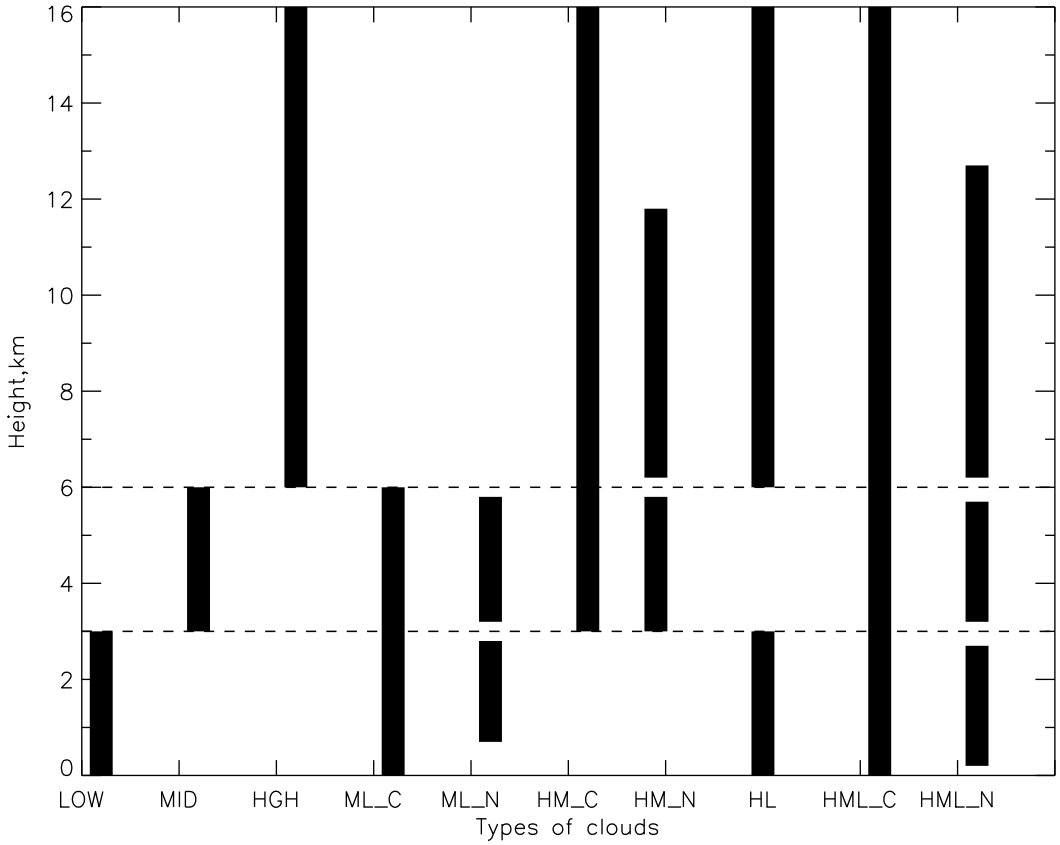

Figure 6. Schematic diagram for categorized clouds by their vertical structures. LOW, single-layered low clouds (<3 km); MID, single-layered middle clouds (3–6 km); HGH, single-layered high clouds (>6 km). C, contiguous clouds; N, noncontiguous clouds. ML, MID over LOW; HM, HGH over MID; and HML, HGN over MID and LOW.

compare their results with this study, their total single- and multilayered CFs would be 23.7% (22.9% + 0.8%) and 25.4% (20.1% + 5.3%) if the 6.1% precipitation fraction was included in their total single- and multilayered CFs. Second, we used a 5 min temporal resolution, while they used a 1 h resolution. From a physical point of view, there are more multilayered cloud occurrences within 1 h than in 5 min. To confirm this further, we plotted Figure 7 using the 10 years of ARM radar-lidar observations. As illustrated in Figure 7 the single-layered CFs decrease from 28.2% in a 5 min resolution to 20% in a 1 h resolution, while the multilayered CFs increase from 20% to 27.7%

4.3. Comparison With GOES Observations

[25] To evaluate the satellite-derived cloud vertical distributions, the highest effective cloud-top distributions retrieved from the GOES data (GOES_TOP) are compared with the ARM radar-derived highest effective cloud-top distributions (radar TOP) over the SGP (Figure 8). The GOES results are averaged from half-hourly observations over a grid box of 0.5° × 0.5°, and the ARM radar results represent the half-hour averages with a 250 m vertical resolution. Since the GOES cloud retrieval algorithms during day and during night are different, we compare the GOES daytime and night results with the ARM radar observations, respectively. During the daytime (Figure 8a) the satellite-retrieved high clouds occur much less frequently than the surface-observed high clouds, while middle and low clouds from GOES are found more often than those from the surface. The frequency of the nighttime GOES high cloud tops (Figure 8b) is in excellent agreement with the highest high cloud tops from the sur-

Table 1. Summary of 10 Categories of Clouds at the Atmospheric Radiation Measurement Program (ARM) Southern Great Plains (SGP) Site (1997–2006)

Cloud Type	Definition	Annual (%)	Spring (%)	Summer (%)	Fall (%)	Winter (%)
1	Single low, <3 km	9.3	10.4	5.0	10.2	11.9
2	Single middle, 3–6 km	2.8	3.3	2.1	2.9	2.8
3	Single high, >6 km	16.7	16.4	19.9	13.7	16.7
4	Middle over low, contiguous	2.4	2.5	1.3	2.5	3.2
5	High over middle, contiguous	3.9	4.3	3.5	3.2	4.8
6	High over both middle and low, contiguous	2.6	2.9	1.8	2.4	3.5
7	Middle over low, noncontiguous	0.8	0.9	0.2	0.9	1.1
8	High over middle, noncontiguous	2.4	3.0	2.5	1.8	2.5
9	High over low, noncontiguous	3.7	4.1	2.1	3.4	5.2
10	High over middle and low, noncontiguous	2.3	2.7	1.3	2.3	3.0
Sum	Total cloud fraction	46.9	50.4	39.8	43.3	54.6

Table 2. Seasonal and Annual Averages of Cloud Fraction (CF) at the ARM SGP Site[a]

	Winter:	Spring:	Summer:	Autumn:	Annual:
	X10/D06/K07	X10/D06/K07	X10/D06/K07	X10/D06/K07	X10/D06/K07
CF_T (%)	54.6/60.6/54.9	50.4/52.6/—	39.8/39.7/42.7	43.3/42.3/—	46.9/48.8/49.1
CF_L (%)	11.9/15.4/8.0	10.4/11.6/—	5.0/4.6/2.3	10.2/10.1/—	9.3/10.4/5.7
CF_M (%)	2.8/3.7/3.3	3.3/4.6/—	2.1/2.3/3.1	2.9/3.7/—	2.8/3.3/3.1
CF_H (%)	16.7/16.9/15.4	16.4/17.0/—	19.9/21.3/14.4	13.7/13.5/—	16.7/17.3/14.1

[a]X10, this study; D06, *Dong et al.* [2006]; K07, *Kollias et al.* [2007]. Note that the single-layered low (CF_L), middle (CF_M), and high (CF_H) CFs in this study and D06 are defined as follows: CF_L is the fraction of time when low clouds ($Z_{top} < 3$ km) occur without clouds above them; CF_H is determined for clouds having a Z_{base} higher than 6 km, with no clouds underneath; and CF_M ranges from 3 to 6 km, without any clouds below or above. K07 used heights of 2 and 6 km to distinguish low, middle, and high clouds and used cloud base height to identify middle clouds. The total CF (CF_T) in K07 is the sum of their total single-layer, multilayer, and precipitation. Note that the sum of CF_T and clear skies is not equal to 100% in K07 because cloud senses of less than 5% were not used in their study. The study periods are 1997–2002 for D06 and from January 1998 to June 2004 for K07. CFs from D06 and this study are derived from the Mace PI product with 5 min temporal resolution, while they are derived from the ARM ARSCL data set with 1 h temporal resolution in K07. The winter season is December–February in this study and D06, while it is November–March in K07.

face observations, but the low clouds occur more often than their surface-observed counterparts.

[26] The CF profiles derived from ARM and GOES observations are calculated using the same method as in Figure 1; that is, CF = FREQ × AWP. For example, the FREQ profiles would be the same as the CF profiles if the AWP values were unity at any altitude. This is nearly true for the ARM observations because the averaged AWP in a 5 min resolution is 92% during the 10 year period (Figure 1b). It is also nearly true for GOES high and middle clouds, but significantly different for low clouds, where their FREQ values are large for both daytime and nighttime results, while their AWP values are small (not shown here), which results in the same CFs as the surface observations as shown in Figures 8c and 8d. The daytime vertical distribution of CF_L from GOES is similar to that for the surface observations for all low clouds, with a slight underestimation in integrated height over the bottom 3 km of the profile. At night the integrated low CF is in better agreement with the uppermost cloud-top values but with a slightly larger underestimate than during the daytime.

[27] The lower frequency and CF of high clouds and higher frequency and CF of middle clouds from GOES relative to the ARM data during daytime are primarily due to three factors. First, H_{eff} is the retrieved radiating height of the cloud, not the physical cloud top. For cirrus clouds the effective radiating height is generally deep within the cloud, so the satellite-retrieved effective radiating height is nor-

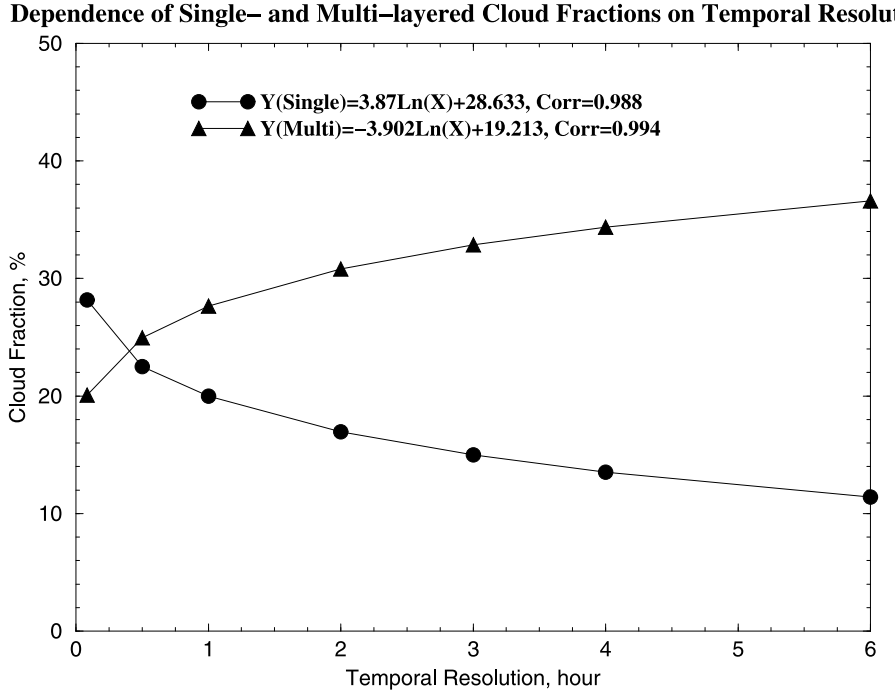

Figure 7. Dependence of single-layered (sum of cloud types 1–3 in Table 1) and multilayered (sum of cloud types 4–10 in Table 1) CFs on different temporal resolutions of the ARM SGP radar-lidar observations during the period 1997–2006.

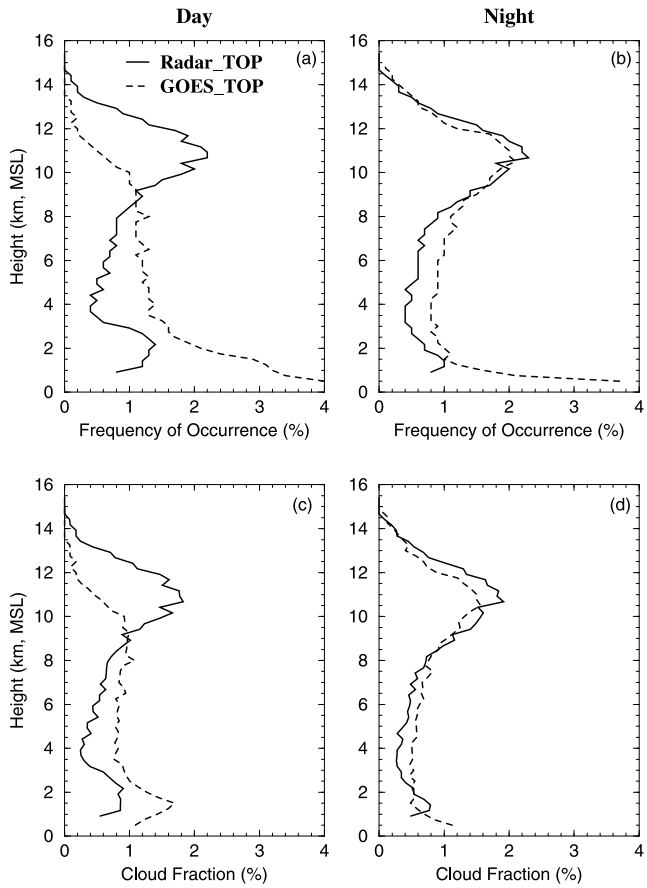

Figure 8. Comparison of the highest cloud-top (a, b) vertical distributions of occurrence and (c, d) fractions derived from GOES and radar-lidar observations over the ARM SGP site, 1998–2006. GOES results are averaged from half-hourly observations over a grid box of 0.5° × 0.5°. ARM radar results represent half-hour averages with a 250 m vertical resolution.

mally about 1–2 km below the physical cloud top [*Minnis et al.*, 1991, 2008b; F. Chang et al., Evaluation of satellite-based upper-troposphere cloud-top height retrievals in multilayer cloud conditions during TC4, submitted to *Journal of Geophysical Research*, 2009]. Second, the ice cloud optical depth from the VISST tends to be overestimated for semitransparent clouds [e.g., *Min et al.*, 2004], so that the cloud radiating temperature (height) will be overestimated (underestimated) for thin cirrus. Third, during the daytime a thin cirrus over a low cloud will be interpreted as a midlevel or low cloud with H_{eff} primarily dependent on the optical depth of the upper cloud. The relatively large difference between the GOES and the radar-derived highest cloud tops at 4 km in Figure 8c suggests that most of the cirrus over low clouds is optically thin.

[28] At night the shapes of the GOES cloud occurrence (Figure 8b) and fraction (Figure 8d) vertical distributions are similar to their ARM counterparts except that the high (midlevel) CFs are slightly lower (higher) than the radar values. This change from the daytime relationships is primarily due to the use of infrared channels only in the SIST. The sensitivity to particle shape in the visible channel retrieval of optical depth, which is a likely source of the overestimate during the day, is gone at night, resulting in more accurate thin cirrus optical depths and H_{eff}. The height of the thin cirrus over low clouds at night is also expected to be much greater than during the day, when the visible optical depth under those conditions is high and no adjustment is made for semitransparency. At night the retrieved optical depth depends on the temperature difference between the high and the low clouds, which is close to that between the high cloud and the surface. Thus, the retrieved cloud tops are often close to the single-layer case, and subsequently, the GOES midlevel CF is much closer to the radar value than during the daytime. These day-night differences are consistent with the single-layer height comparisons performed by *Smith et al.* [2008].

[29] The vertical profiles of GOES low-cloud occurrence frequencies and fractions change significantly from day to night. Although the FREQ is quite high for the lowest height bins, the AWP is low, resulting in a peak at 1.38 km during daytime and a more uniform fraction distribution at night. The small values of AWP and large values of FREQ in the lowest bin could be due to small cumulus clouds or fog patches during the day and fog patches and noise in the brightness temperature differences at night. The latter would result in small AWP values with temperatures close to the surface value. *Dong et al.* [2008] and *Smith et al.* [2008] found that the average VISST low-cloud-top heights were 0.1 to 0.5 km less than the radar values, which are similar to those in Figure 8.

5. Summary and Concluding Remarks

[30] Analysis of a decade of nearly continuous ARM radar-lidar and GOES satellite observations at the ARM SCF has yielded the following conclusions.

1. There is excellent agreement in surface and GOES-based, long-term mean CFs, which are independent of temporal resolution and spatial scales. Cloud FREQ increases and AWP decreases with increasing averaging time and spatial scales. Computed over a 0.5 h period, FREQ and AWP derived from the ARM radar-lidar data agree very well with the same quantities determined from GOES for a 0.5° region centered on the ARM SGP site. Similarly, the 4 h surface averages are comparable to those derived from GOES for a 2.5° grid box. Thus, when comparing clouds from weather or climate models to the SGP cloud data, the temporal averaging time should be matched to the size of the model resolution. Empirical functions developed here for that purpose are unlikely to be useful for model regions much larger than 2.5° because that is the upper limit of regional size that was considered.

2. The vertical distributions of FREQ, AWP, and CF derived from the ARM radar-lidar observations are similar to those given in Figure 1; that is, FREQ values increase and AWP values decrease, but CF values remain constant from 5 min to 6 h averaging periods. However, the CF increases at any altitude as the vertical resolution increases from 90 to 1000 m. The CF profiles are characterized by distinct bimodal vertical distributions having a lower peak between 1 and 2 km and a higher one between 8 and 11 km. The 10-year mean total CF, 46.9%, varies seasonally from a

summer minimum of 39.8% to a maximum of 54.6% during the winter.

3. The CFs are also compared with those in other studies [e.g., *Dong et al.*, 2006; *Kollias et al.*, 2007; and *Mace and Benson*, 2008] to determine how well the results analyzed in this study represent the cloud climatology at the ARM SCF. Although the total CFs in D06, K07, and MB08 were derived from different data sets and time periods, they have almost the same annual mean, ~48%–49%, which is about 1%–2% higher than that in this study. This apparent discrepancy results from the inclusion of data from 2005 and 2006, when the total CFs in 2005 and 2006 were approximately 41%. More clouds occurred during the winter seasons of 1997–2002 than in the winters of 2003–2006, mostly due to fewer single- layered low clouds during the latter period. The differences in single- and multilayered CFs between K07 and this study can be explained by the different temporal resolutions used in these two studies, where single-layered CFs decrease but multilayered CFs increase from a 5 min to a 1 h resolution.

4. The vertical distribution of nighttime GOES high cloud tops agrees well with surface observations, but during the daytime there are fewer high clouds than seen from the surface observations. The FREQ for both daytime and nighttime GOES low cloud tops are significantly higher than that from surface observations, but the CFs are in good agreement.

[31] These results should provide the most complete statistics to date of the long-term average CF and vertical distributions of clouds over the climatically important SGP site. These statistics can be used as ground truth for both surface observers and satellite researchers to quantitatively understand and explain the differences between their observations and cloud truth. They should also be valuable for advancing our understanding of the vertical distributions of clouds and for enabling climate and forecast modelers to evaluate their simulations more fully and improve their parameterizations over the SGP Central Facility. Comparisons between the satellite and the surface data indicate the areas of needed improvement in the satellite retrievals, particularly in the area of multilayered cloud detection. The results presented here represent only one region on the globe and may not necessarily represent the spatial and temporal interchangeability of cloud cover in other areas, such as coastal stations, where long-term spatial gradients are likely.

[32] **Acknowledgments.** The authors thank Gerald G. Mace and Sally Benson of the University of Utah for providing their PI product. This research was primarily supported by the NASA MAP project under grant NNG06GB59G at the University of North Dakota and by the Office of Science (BER), U.S. Department of Energy, Interagency Agreement DE-AI02-08ER64546. The University of North Dakota authors were also supported by the NASA CERES project under grant NNL04AA11G, the NASA NEWS project under grant NNX07AW05G, and the NSF under grant ATM0649549.

References

Ackerman, T. P., and G. M. Stokes (2003), The Atmospheric Radiation Measurement Program, *Phys. Today*, *56*, 38–44, doi:10.1063/1.1554135.

Benjamin, S. G., et al. (2004), An hourly assimilation/forecast model: The RUC, *Mon. Weather Rev.*, *113*, 495–518, doi:10.1175/1520-0493(2004)132<0495:AHACTR>2.0.CO;2.

Chang, F., and Z. Li (2005), A near-global climatology of single-layer and overlapped clouds and their optical properties from Terra/MODIS data using a new algorithm, *J. Clim.*, *18*, 4752–4771, doi:10.1175/JCLI3553.1.

Clothiaux, E. E., K. P. Moran, B. E. Martner, T. P. Ackerman, G. G. Mace, T. Uttal, J. H. Mather, K. B. Widener, M. A. Miller, and D. J. Rodriguez (1999), The Atmospheric Radiation Measurement Program cloud radars: Operational modes, *J. Atmos. Oceanic Technol.*, *16*, 819–827, doi:10.1175/1520-0426(1999)016<0819:TARMPC>2.0.CO;2.

Clothiaux, E. E., T. P. Ackerman, G. G. Mace, K. P. Moran, R. T. Marchand, M. A. Miller, and B. E. Martner (2000), Objective determination of cloud heights and radar reflectivities using a combination of active remote sensors at the Atmospheric Radiation Measurement Program Cloud and Radiation Test Bed (ARM CART) sites, *J. Appl. Meteorol.*, *39*, 645–665, doi:10.1175/1520-0450(2000)039<0645:ODOCHA>2.0.CO;2.

Dong, X., P. Minnis, G. G. Mace, W. L. Smith Jr., M. Poellot, R. Marchand, and A. Rapp (2002), Comparison of stratus cloud properties deduced from surface, GOES, and aircraft data during the March 2000 ARM Cloud IOP, *J. Atmos. Sci.*, *59*, 3265–3284, doi:10.1175/1520-0469(2002)059<3265:COSCPD>2.0.CO;2.

Dong, X., P. Minnis, and B. Xi (2005), A climatology of midlatitude continental clouds from the ARM SGP Central Facility: Part I. Low-level cloud macrophysical, microphysical, and radiative properties, *J. Clim.*, *18*, 1391–1410, doi:10.1175/JCLI3342.1.

Dong, X., B. Xi, and P. Minnis (2006), A climatology of midlatitude continental clouds from the ARM SGP Central Facility: Part II. Cloud fraction and surface radiative forcing, *J. Clim.*, *19*, 1765–1783, doi:10.1175/JCLI3710.1.

Dong, X., P. Minnis, B. Xi, S. Sun-Mack, and Y. Chen (2008), Validation of CERES-MODIS stratus cloud properties using ground-based measurements at the DOE ARM SGP site, *J. Geophys. Res.*, *113*, D03204, doi:10.1029/2007JD008438.

Hogan, R. J., and A. J. Illingworth (2000), Deriving cloud overlap statistics from radar, *Q. J. R. Meteorol. Soc.*, *126*, 2903–2909, doi:10.1002/qj.49712656914.

Hogan, R. J., C. Jakob, and A. J. Illingworth (2001), Comparison of ECMWF winter-season cloud fraction with radar-derived values, *J. Atmos. Meteorol*, *40*, 513–525, doi:10.1175/1520-0450(2001)040<0513:COEWSC>2.0.CO;2.

Illingworth, A. J., et al. (2007), CLOUDNET, continuous evaluation of cloud profiles in seven operational models using ground-based observations, *Bull. Am. Meteorol. Soc.*, *88*, 883–898, doi:10.1175/BAMS-88-6-883.

Kennedy, A. D., X. Dong, B. Xi, P. Minnis, A. Del Genio, A. B. Wolf, and M. M. Khaiyer (2010), Evaluation of the NASA GISS single column model simulated clouds using combined surface and satellite observations, *J. Clim.*, doi:10.1175/2010JCLI3353.1, in press.

Kim, B. G., S. A. Klein, and J. R. Norris (2005), Continental liquid water cloud variability and its parameterization using Atmospheric Radiation Measurement data, *J. Geophys. Res.*, *110*, D15S08, doi:10.1029/2004JD005122.

Kollias, P., G. Tselioudis, and B. A. Albrecht (2007), Cloud climatology at the southern great plains and the layer structure, drizzle, and atmospheric modes of continental stratus, *J. Geophys. Res.*, *112*, D09116, doi:10.1029/2006JD007307.

Mace, G. G., and S. Benson (2008), The vertical structure of cloud occurrence and radiative forcing at the SGP ARM site as revealed by 8 years of continuous data, *J. Clim.*, *21*, 2591–2610, doi:10.1175/2007JCLI1987.1.

Mace, G. G., and S. Benson-Troth (2002), Cloud-layer overlap characteristics derived from long-term cloud radar data, *J. Clim.*, *15*, 2505–2515, doi:10.1175/1520-0442(2002)015<2505:CLOCDF>2.0.CO;2.

Mace, G. G., et al. (2006), Cloud radiative forcing at the Atmospheric Radiation Measurement Program Climate Research Facility: 1. Technique, validation, and comparison to satellite-derived diagnostic quantities, *J. Geophys. Res.*, *111*, D11S90, doi:10.1029/2005JD005921.

Min, Q., P. Minnis, and M. M. Khaiyer (2004), Comparison of cirrus optical depths from GOES-8 and surface measurements, *J. Geophys. Res.*, *109*, D20119, doi:10.1029/2003JD004390.

Minnis, P., P. W. Heck, and E. F. Harrison (1991), The 27–28 October 1986 FIRE IFO Case Study: Cloud parameter fields derived from satellite data, *Mon. Weather Rev.*, *118*, 2426–2446, doi:10.1175/1520-0493(1990)118<2426:TOFICC>2.0.CO;2.

Minnis, P., et al. (2008a), Cloud detection in non-polar regions for CERES using TRMM VIRS and Terra and Aqua MODIS data, *IEEE Trans. Geosci. Remote Sens.*, *46*, 3857–3884, doi:10.1109/TGRS.2008.2001351.

Minnis, P., C. Yost, S. Sun-Mack, and Y. Chen (2008b), Estimating the top altitude of optically thick ice clouds from thermal infrared satellite observations using CALIPSO data, *Geophys. Res. Lett.*, *35*, L12801, doi:10.1029/2008GL033947.

Moran, K. P., B. E. Martner, M. J. Post, R. A. Kropfli, D. C. Welsh, and K. B. Widener (1998), An unattended cloud-profiling radar for use in climate research, *Bull. Am. Meteorol. Soc.*, *79*, 443–455, doi:10.1175/1520-0477(1998)079<0443:AUCPRF>2.0.CO;2.

Naud, C. M., A. Del Genio, G. G. Mace, S. Benson, E. E. Clothiaux, and P. Kollias (2008), Impact of Dynamics and Atmospheric State on Cloud Vertical Overlap, *J. Clim.*, *21*, 1758–1770, doi:10.1175/2007JCLI1828.1.

Smith, W. L., P. Minnis, H. Finney, R. Palikonda, and M. M. Khaiyer (2008), An evaluation of operational GOES-derived single-layer cloud top heights with ARSCL over the ARM Southern Great Plains site, *Geophys. Res. Lett.*, *35*, L13820, doi:10.1029/2008GL034275.

Solomon, S., D. Qin, M. Manning, M. Marquis, K. Averyt, M. M. B. Tignor, H. L. Mille Jr., and Z. Chen (Eds.) (2007), *Climate Change 2007: The Physical Science Basis*, Cambridge Univ. Press., Cambridge, U. K.

Stephens, G. L., et al. (2002), The cloudsat mission and the A-train, *Bull. Am. Meteorol. Soc.*, *83*, 1771–1790, doi:10.1175/BAMS-83-12-1771.

Trepte, Q., P. Minnis, and R. F. Arduini (2002), Daytime and nighttime polar cloud and snow identification using MODIS data, *Proc. SPIE 3rd Int. Asia-Pacific Environ. Remote Sensing Symp.: Remote Sensing of Atmosphere, Ocean, Environment, and Space*, Hangzhou, China, 23–27 October, Vol. 4891, pp. 449–459.

Warren, S. G., C. J. Hahn, J. London, R. M. Chervin, and R. L. Jenne (1984), Atlas of simultaneous occurrence of different cloud types over land, *NCAR Tech. Note*, NCAR/TN-241+STR, 209 pp., National Center for Atmospheric Research, Boulder, Colo.

Wielicki, B. A., R. D. Cess, M. D. King, D. A. Randall, and E. F. Harrison (1995), Mission to Planet Earth: Role of clouds and radiation in climate, *Bull. Am. Meteorol. Soc.*, *76*, 2125–2153, doi:10.1175/1520-0477(1995)076<2125:MTPERO>2.0.CO;2.

Zhang, M. H., et al. (2005), Comparing clouds and their seasonal variations in 10 atmospheric genergal circulation models with satellite measurements, *J. Geophys. Res.*, *110*, D15S02, doi:10.1029/2004JD005021.

X. Dong and B. Xi, University of North Dakota, Grand Forks, ND 58202, USA. (baike@aero.und.edu)

M. M. Khaiyer and P. Minnis, NASA Langley Research Center, Hampton, VA 23681-2199, USA.